Electronic Supplementary Information

A series of five-coordinated copper coordination polymers for efficient degradation of organic dyes under visible light irradiation

Lu-Lu Shi, Tian-Rui Zheng, Min Li, Lin-Lu Qian, Bao-Long Li*, Hai-Yan Li

State and Local Joint Engineering Laboratory for Functional Polymeric Materials, College of Chemistry, Chemical Engineering and Materials Science, Soochow University, Suzhou 215123, P.R. China.

Table S1. Crystallographic data for **1**, **2**, **3, 4** and **5**.

	1	**2**	**3**	**4**	**5**
Formula	$C_{50}H_{54}Cu_4N_8O_{19}$	$C_{32}H_{26}Cu_2N_4O_8$	$C_{34}H_{30}Cu_2N_4O_8$	$C_{36}H_{34}Cu_2N_4O_9$	$C_{38}H_{39}Cu_2N_8O_{11}$
Fw	1325.17	721.65	749.70	793.75	910.85
T/K	223(2)	223(2)	293(2)	223(2)	253(2)
Crystal system	Triclinic	Triclinic	Triclinic	Monoclinic	Triclinic
Space group	$P\bar{1}$	$P\bar{1}$	$P\bar{1}$	$C2/c$	$P\bar{1}$
a/Å	10.1526(11)	10.8971(5)	9.4520(6)	10.2620(3)	9.7731(6)
b/Å	11.2399(8)	10.9070(6)	12.2857(8)	21.1852(5)	9.8545(7)
c/Å	11.9600(13)	13.6446(4)	13.6945(10)	15.7859(4)	22.5635(9)
α (°)	88.231(7)	78.060(4)	93.448(6)	90	86.079(4)
β (°)	88.556(9)	77.934(3)	94.362(6)	97.520(3)	88.972(4)
γ (°)	82.101(7)	79.380(4)	94.392(5)	90	68.582(6)
V /Å^3	1350.9(2)	1534.64(12)	1577.52(19)	3402.37(15)	2018.2(2)
F(000)	674	736	768	1624	938
Z	1	2	4	4	2
ρ_{calcd} (g cm^{-3})	1.629	1.562	1.578	1.550	1.499
μ(mm^{-1})	1.636	1.444	1.408	2.072	1.123
Reflections collected	10946	13595	15119	6089	19921
Unique reflections	5754 (R(int) = 0.0468)	6571 [R(int) = 0.0372]	6799 [R(int) = 0.0335]	2999 [R(int) = 0.0316]	8636 [R(int) = 0.0412]
Parameter	394	417	435	286	535
Goodness of fit	1.004	1.052	1.021	1.044	1.091
R_1 [I > 2σ(I)]	0.0555	0.0401	0.0402	0.0460	0.0735
wR_2 (all data)	0.1362	0.0902	0.1008	0.1299	0.2084

Table S2. Selected bond lengths (Å) and angles (°) for **1**, **2**, **3, 4** and **5**.

		1	
Cu1-O1A	1.970(3)	Cu1-O3B	1.953(3)
Cu1-O7	1.877(3)	Cu1-N1	1.986(4)
Cu2-O2A	1.977(3)	Cu2-O5	2.022(3)
Cu2-O7	1.883(3)	Cu2-O8	2.337(4)
Cu2-N3C	1.965(4)		
O1A-Cu1-O3B	84.64(14)	O1A-Cu1-O7	92.24(14)
O1A-Cu1-N1	158.67(16)	O3B-Cu1-O7	170.99(14)
O3B-Cu1-N1	89.86(15)	O7-Cu1-N1	95.98(14)

O2A-Cu2-O5	178.23(14)	O2A-Cu2-O7	93.06(13)
O2A-Cu2-O8	85.29(14)	O2A-Cu2-N3C	86.63(14)
O5-Cu2-O7	88.46(12)	O5-Cu2-O8	95.21(12)
O5-Cu2-N3C	91.67(14)	O7-Cu2-O8	104.02(15)
O7-Cu2-N3C	166.12(15)	O8-Cu2-N3C	89.78(16)

2

Cu1-O1	1.9653(19)	Cu1-O2A	1.9948(18)
Cu1-O5	1.9724(17)	Cu1-O6A	1.9906(18)
Cu1-N1	2.129(2)	Cu2-O3C	1.991(2)
Cu2-O4D	1.989(2)	Cu2-O7	1.9707(17)
Cu2-O8B	1.9706(16)	Cu2-N3	2.131(2)
O1-Cu1-O2A	166.28(9)	O1-Cu1-O5	86.23(9)
O1-Cu1-O6A	88.51(9)	O1-Cu1-N1	96.94(9)
O2A-Cu1-O5	93.94(8)	O2A-Cu1-O6A	88.08(8)
O2A-Cu1-N1	96.67(9)	O5-Cu1-O6A	165.86(9)
O5-Cu1-N1	96.54(9)	O6A-Cu1-N1	97.12(8)
O3B-Cu2-O4D	166.69(9)	O3B-Cu2-O7	89.43(9)
O3B-Cu2-O8C	90.76(9)	O3B-Cu2-N3	89.99(9)
O4D-Cu2-O7	88.86(9)	O4D-Cu2-O8C	87.72(8)
O4D-Cu2-N3	103.30(9)	O7-Cu2-O8C	165.90(8)
O7-Cu2-N3	101.34(8)	O8C-Cu2-N3	92.76(8)

3

Cu1-O1	1.978(2)	Cu1-O2A	1.9834(19)
Cu1-O5	1.9910(19)	Cu1-O6A	1.965(2)
Cu1-N2	2.149(2)	Cu2-O3	2.373(3)
Cu2-O4	1.934(2)	Cu2-O7C	2.028(2)
Cu2-O8B	1.964(2)	Cu2-N4	1.945(3)
O1-Cu1-O2A	165.45(9)	O1-Cu1-O5	88.56(10)
O6A-Cu1-O1	88.79(10)	O1-Cu1-N2	96.13(9)
O2A-Cu1-O5	89.43(9)	O6A-Cu1-O2A	89.50(10)
O2A-Cu1-N2	98.40(9)	O6A-Cu1-O5	165.26(8)
O5-Cu1-N2	94.38(9)	O6A-Cu1-N2	100.32(9)
O4-Cu2-O3	59.49(8)	O7C-Cu2-O3	90.03(11)
O8B-Cu2-O3	127.79(12)	N4-Cu2-O3	108.49(10)
O4-Cu2-O7C	93.32(12)	O4-Cu2-O8B	91.33(10)
O4-Cu2-N4	167.38(10)	O8B-Cu2-O7C	137.44(15)
N4-Cu2-O7C	90.39(13)	N4-Cu2-O8B	94.08(11)

4

Cu1-O1	1.981(2)	Cu1-O2A	1.996(2)
Cu1-O3	1.962(2)	Cu1-O4A	1.968(2)
Cu1-N1	2.117(5)		
O1-Cu1-O2A	166.11(11)	O1-Cu1-O3	87.95(11)
O1-Cu1-O4A	92.02(12)	O1-Cu1-N1	82.8(2)
O2A-Cu1-O3	88.49(11)	O2A-Cu1-O4A	88.28(12)

O2A-Cu1-N1	110.7(2)	O3-Cu1-O4A	166.29(9)
O3-Cu1-N1	91.27(19)	O4A-Cu1-N1	102.34(19)
		5	
Cu1-O1	1.965(3)	Cu1-O7	1.942(3)
Cu1-O9	2.294(5)	Cu1-N4A	1.971(4)
Cu1-N7	2.008(4)	Cu2-O3	2.129(4)
Cu2-O5B	1.990(4)	Cu2-N2	2.018(4)
Cu2-N6	1.966(4)	Cu2-N8B	2.008(4)
O1-Cu1-O7	175.02(16)	O1-Cu1-O9	92.86(18)
O1-Cu1-N4A	90.21(15)	O1-Cu1-N7	81.91(15)
O7-Cu1-O9	90.24(18)	O7-Cu1-N4A	93.25(16)
O7-Cu1-N7	94.23(16)	O9-Cu1-N4A	97.44(17)
O9-Cu1-N7	89.46(17)	N4A-Cu1-N7	169.80(17)
O3-Cu2-O5B	118.6(2)	O3-Cu2-N2	92.1(3)
O3-Cu2-N6	96.79(18)	O3-Cu2-N8B	89.01(18)
O5B-Cu2-N2	148.9(3)	O5B-Cu2-N6	90.73(17)
O5B-Cu2-N8B	81.04(17)	N2-Cu2-N6	90.9(2)
N2-Cu2-N8B	95.1(2)	N6-Cu2-N8B	171.51(18)

Symmetry transformations used to generate equivalent atoms: A x, -1+y, z; B 2-x, -y, 1-z; C 1+x, -1+y, z for **1**; A –x, 1-y, 1-z; B 1-x, -y, -z; C 1-x, -y, 1-z; D x, y, -1+z for **2**; A -x+1, -y+1, -z+1; B -x, -y, -z+1; C x, y, z+1 for **3**; A 1-x, 1-y, 1-z for **4**; A –x, -y+3, -z+1; B x, y-1, z for **5**

Table S3. Hydrogen bonds for **1** and **5** (Å and °).

D-H···A	d(D-H)	d(H···A)	D(D···A)	<(DHA)
		1		
O(7)-H(1W)···O(4)	0.88(2)	1.93(3)	2.781(4)	164(6)
O(8)-H(2W)···O(9)^{i}	0.841(19)	2.03(2)	2.865(6)	172(6)
O(8)-H(3W)···O(6)	0.85(2)	1.90(3)	2.692(5)	156(5)
O(9)-H(4W)···O(6)	0.89(2)	1.90(3)	2.784(6)	168(7)
		5		
O(9)-H(1W)···O(1)^{i}	0.89(2)	2.06(4)	2.877(6)	153(7)
O(9)-H(2W)···O(12)	0.90(2)	1.75(3)	2.619(17)	163(6)
O(10)-H(4W)···O(5)	0.92(2)	2.33(5)	3.198(11)	157(11)

Symmetry transformations used to generate equivalent atoms: i -x+2, -y, -z+2 for **1**; i –x, -y+4, -z+1 for **5**.

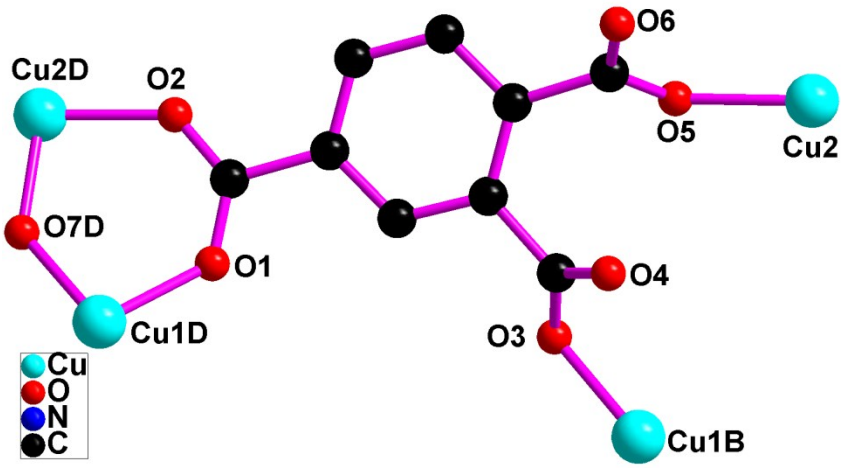

Fig. S1 Each 1,2,4-btc ligand connects four Cu(II) atoms in **1**.

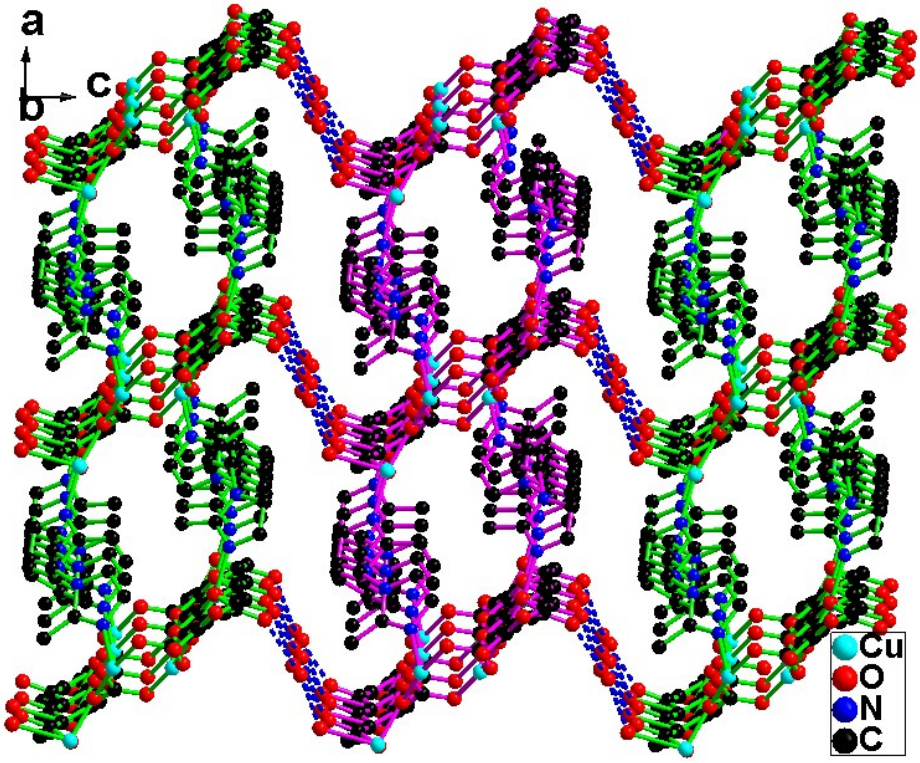

Fig. S2 The 3D hydrogen bonding network in **1**.

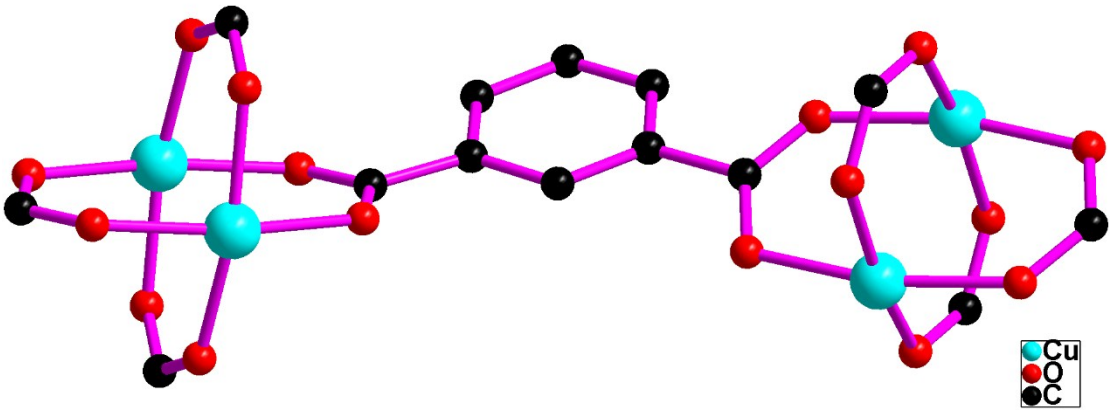

Fig. S3 The coordination mode of ip ligand in **2**.

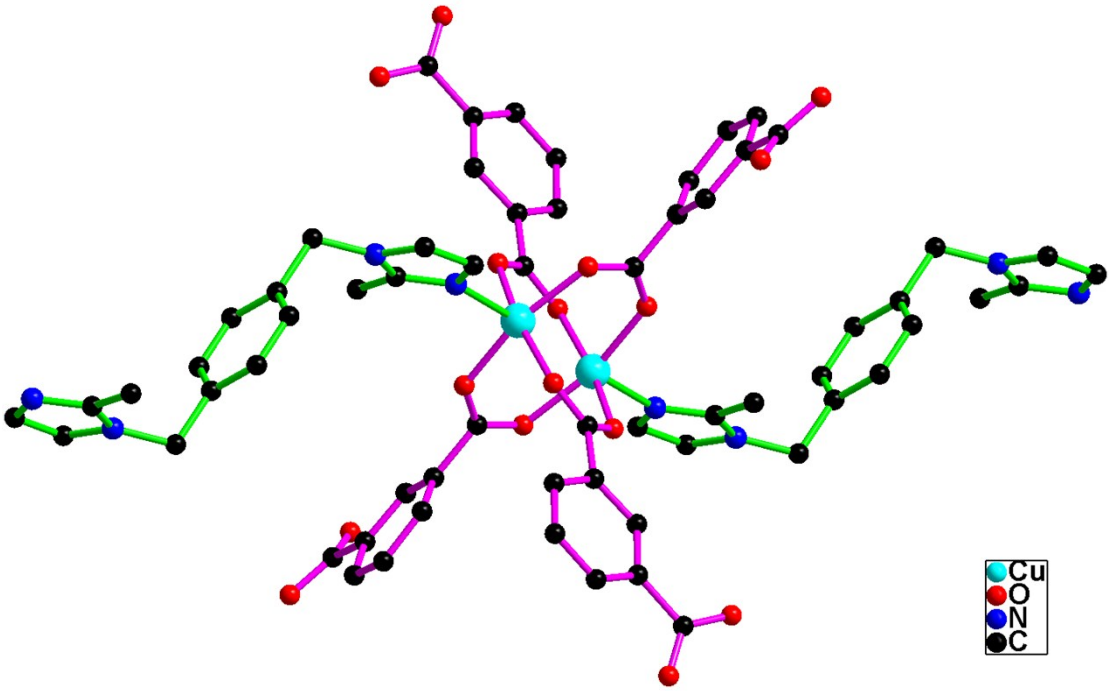

Fig. S4 The 6-connected $[Cu_2(COO)_4]$ dimer in **2**.

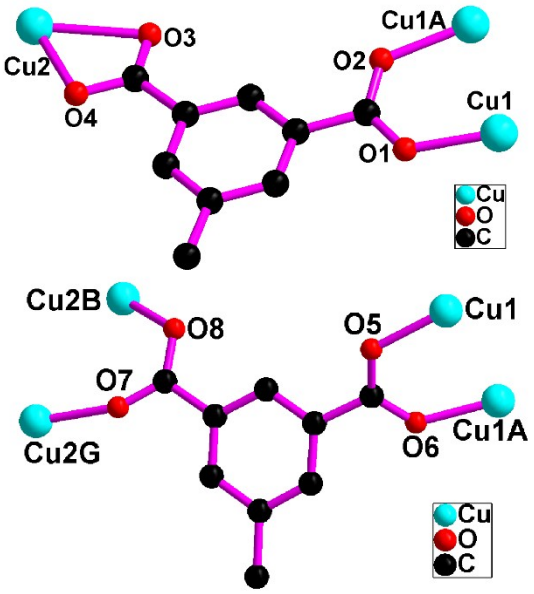

Fig. S5 The coordination mode of two kinds of Meip ligands in **3**.

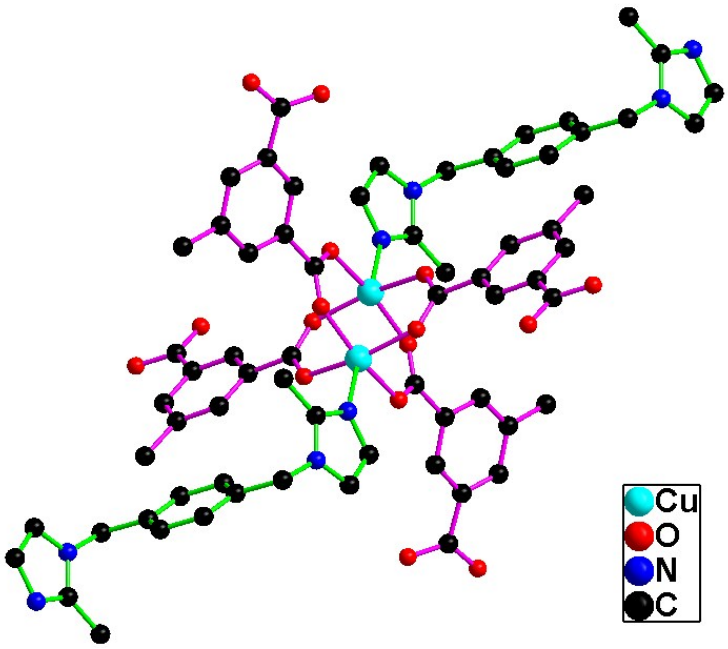

Fig. S6 The 6-connected $[Cu_2(COO)_4]$ dimer in **3**.

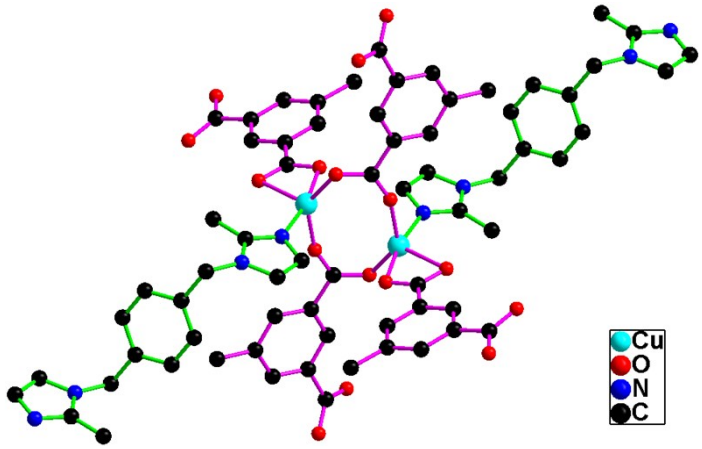

Fig. S7 The 6-connected $[Cu_2(COO)_2]$ dimer in **3**.

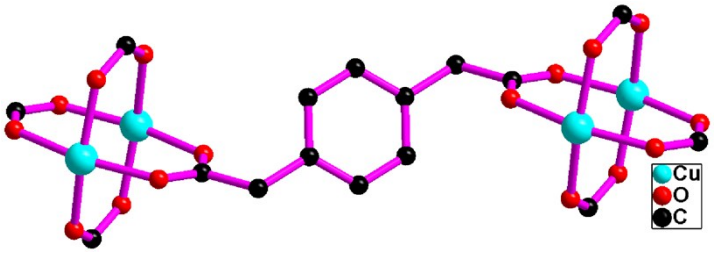

Fig. S8 The coordination mode of pbda ligand in **4**.

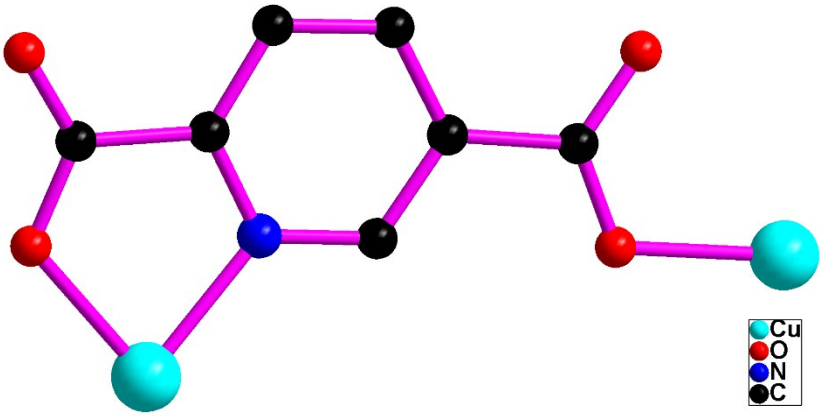

Fig. S9 The coordination mode of 2,5-pydc ligand in **5**.

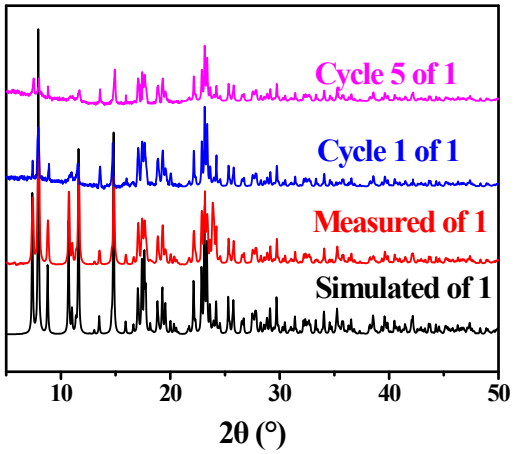

Fig. S10 PXRD patterns of the measured, simulated and after photocatalytic degradation of the MO solution of **1** for example.

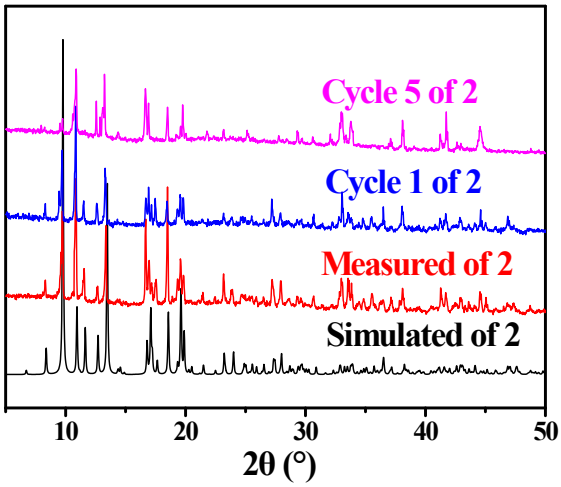

Fig. S11 PXRD patterns of the measured, simulated and after photocatalytic degradation of the MO solution of **2** for example.

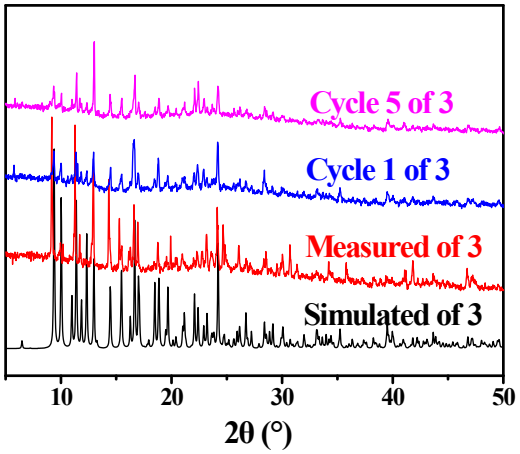

Fig. S12 PXRD patterns of the measured, simulated and after photocatalytic degradation of the MO solution of **3** for example.

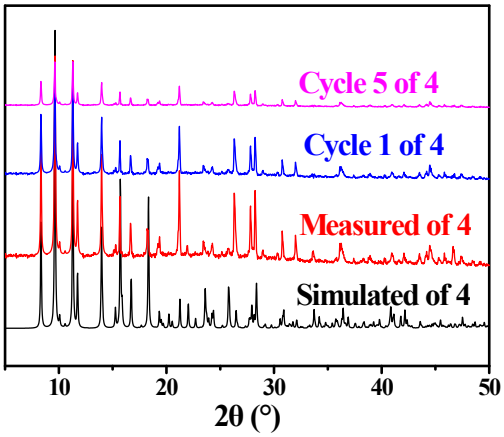

Fig. S13 PXRD patterns of the measured, simulated and after photocatalytic degradation of the MO solution of **4** for example.

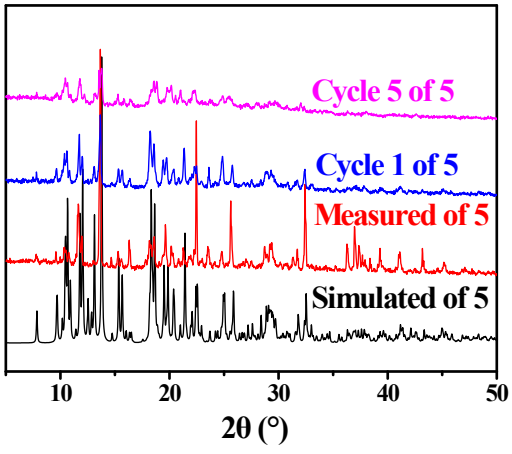

Fig. S14 PXRD patterns of the measured, simulated and after photocatalytic degradation of the MO solution of **5** for example.

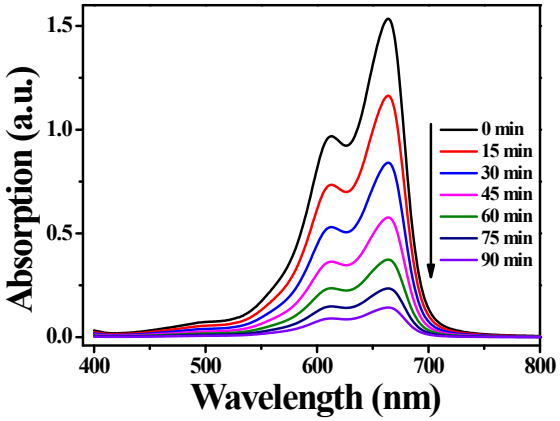

Fig. S15 The UV-vis absorption spectra of MB solution during photocatalytic degradation of the MB solution using catalyst **2** in the presence of H_2O_2 under visible light irradiation.

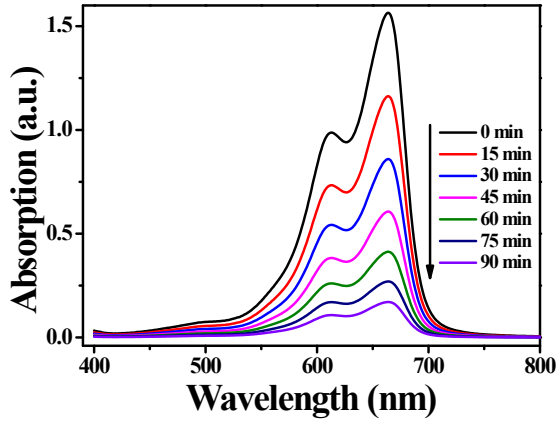

Fig. S16 The UV-vis absorption spectra of MB solution during photocatalytic degradation of the MB solution using catalyst **3** in the presence of H_2O_2 under visible light irradiation.

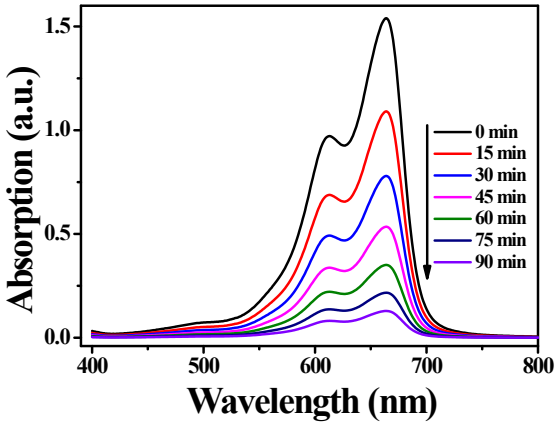

Fig. S17 The UV-vis absorption spectra of MB solution during photocatalytic degradation of the MB solution using catalyst **4** in the presence of H_2O_2 under visible light irradiation.

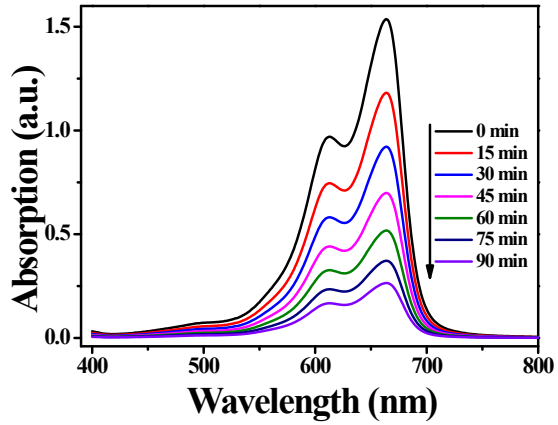

Fig. S18 The UV-vis absorption spectra of MB solution during photocatalytic degradation of the MB solution using catalyst **5** in the presence of H_2O_2 under visible light irradiation.

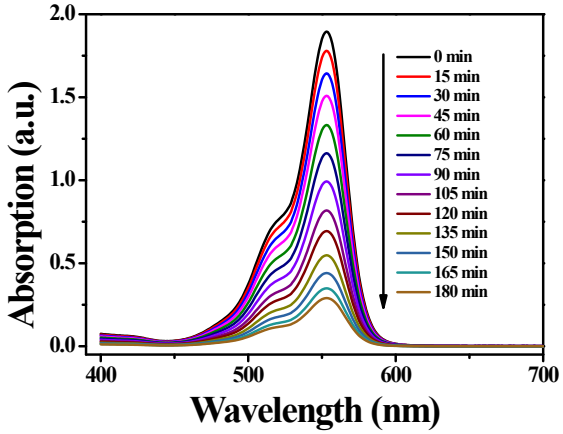

Fig. S19 The UV-vis absorption spectra of RhB solution during photocatalytic degradation of the RhB solution using catalyst **2** in the presence of H_2O_2 under visible light irradiation.

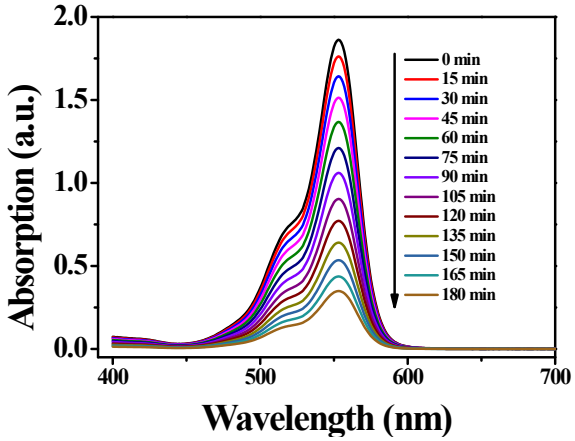

Fig. S20 The UV-vis absorption spectra of RhB solution during photocatalytic degradation of the RhB solution using catalyst **3** in the presence of H_2O_2 under visible light irradiation

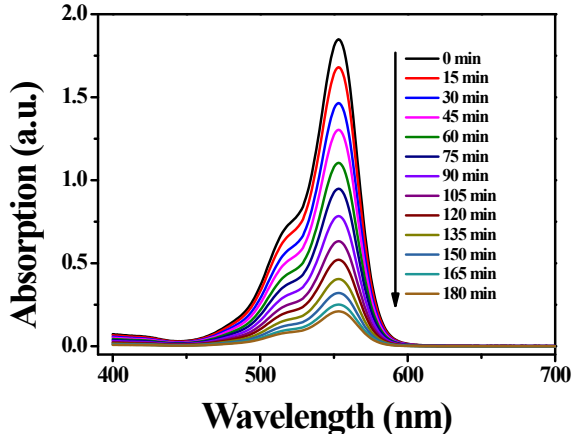

Fig. S21 The UV-vis absorption spectra of RhB solution during photocatalytic degradation of the RhB solution using catalyst **4** in the presence of H_2O_2 under visible light irradiation

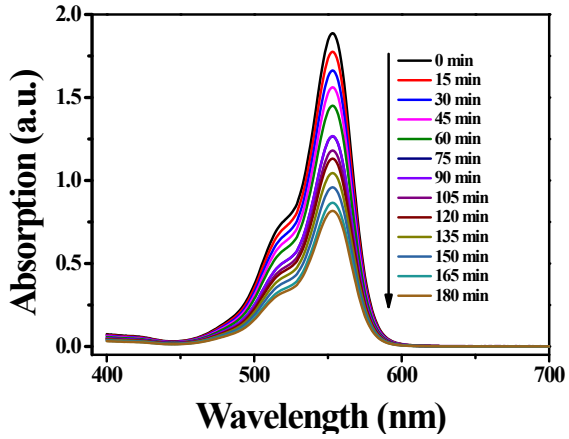

Fig. S22 The UV-vis absorption spectra of RhB solution during photocatalytic degradation of the RhB solution using catalyst **5** in the presence of H_2O_2 under visible light irradiation

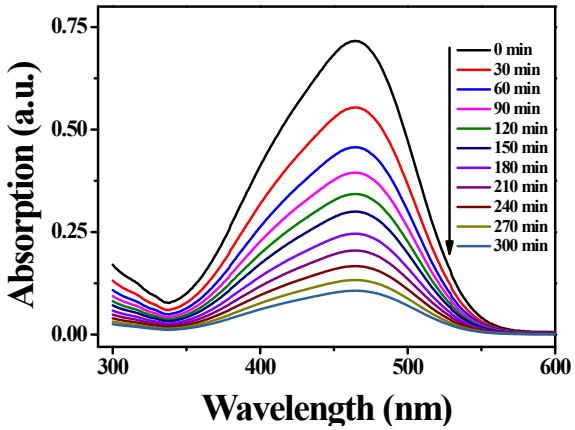

Fig. S23 The UV-vis absorption spectra of MO solution during photocatalytic degradation of the MO solution using catalyst **2** in the presence of H_2O_2 under visible light irradiation

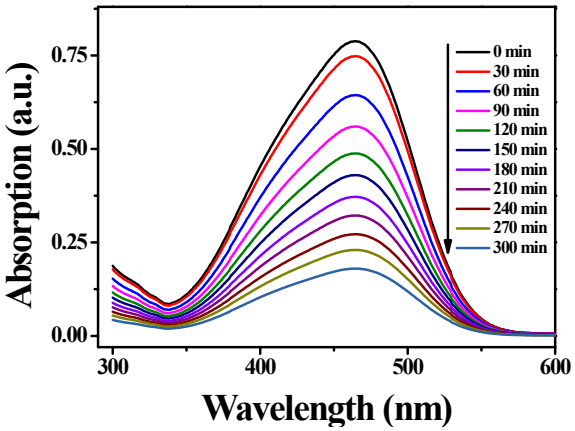

Fig. S24 The UV-vis absorption spectra of MO solution during photocatalytic degradation of the MO solution using catalyst **3** in the presence of H_2O_2 under visible light irradiation

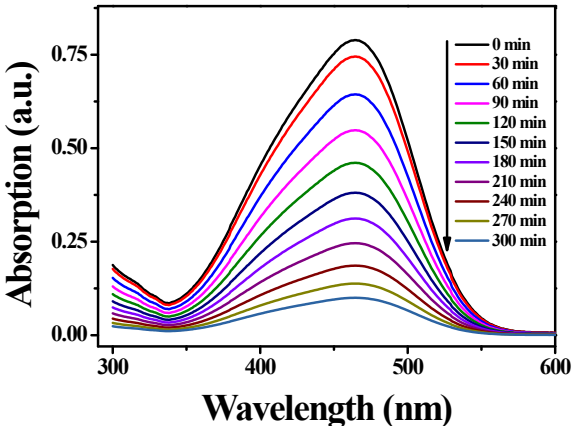

Fig. S25 The UV-vis absorption spectra of MO solution during photocatalytic degradation of the MO solution using catalyst **4** in the presence of H_2O_2 under visible light irradiation

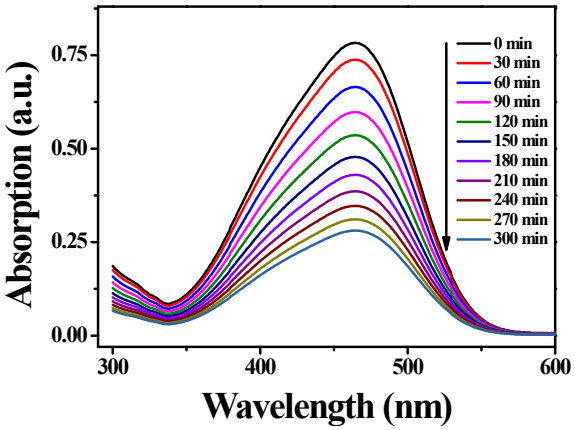

Fig. S26 The UV-vis absorption spectra of MO solution during photocatalytic degradation of the MO solution using catalyst **5** in the presence of H_2O_2 under visible light irradiation

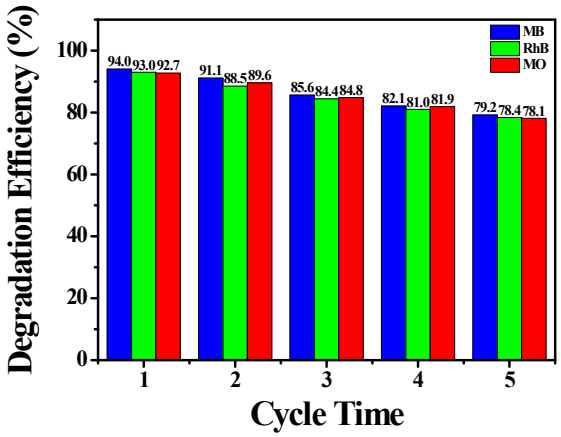

Fig. S27 Photocatalytic efficiencies of degradation of MB, RhB and MO using catalysts **1** in the in the presence of H_2O_2 under visible light irradiation in catalytic cycle 1 to cycle 5.

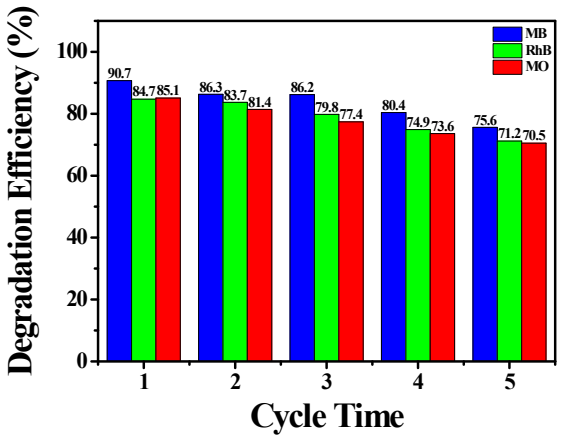

Fig. S28 Photocatalytic efficiencies of degradation of MB, RhB and MO using catalysts **2** in the in the presence of H_2O_2 under visible light irradiation in catalytic cycle 1 to cycle 5.

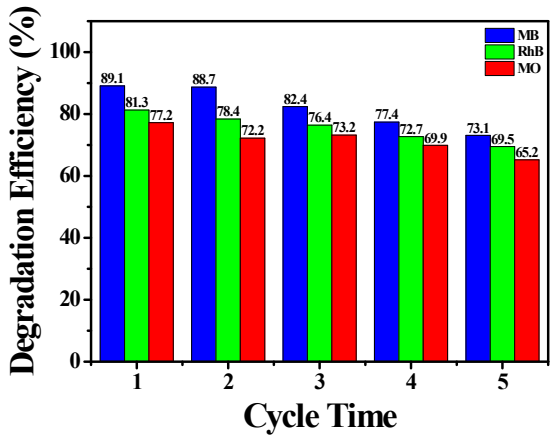

Fig. S29 Photocatalytic efficiencies of degradation of MB, RhB and MO using catalysts **3** in the in the presence of H_2O_2 under visible light irradiation in catalytic cycle 1 to cycle 5.

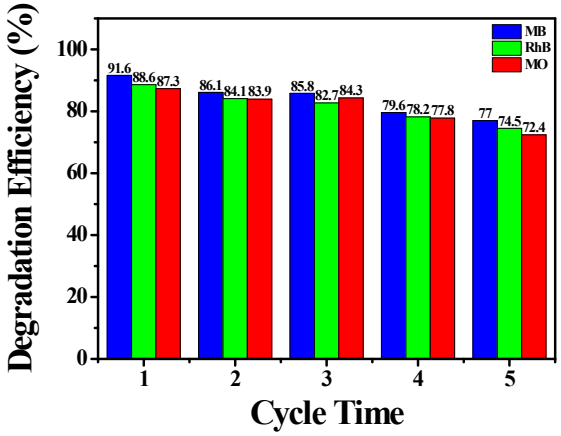

Fig. S30 Photocatalytic efficiencies of degradation of MB, RhB and MO using catalysts **4** in the in the presence of H_2O_2 under visible light irradiation in catalytic cycle 1 to cycle 5.

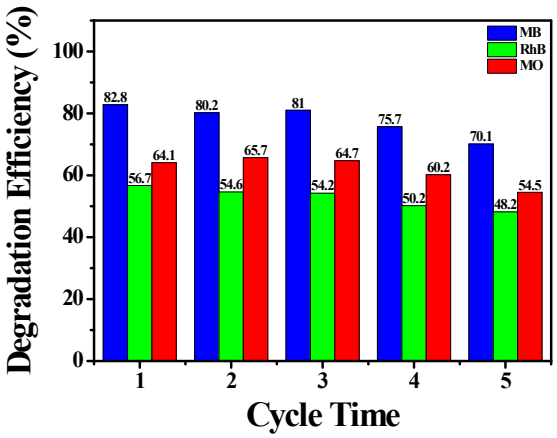

Fig. S31 Photocatalytic efficiencies of degradation of MB, RhB and MO using catalysts **5** in the in the presence of H_2O_2 under visible light irradiation in catalytic cycle 1 to cycle 5.

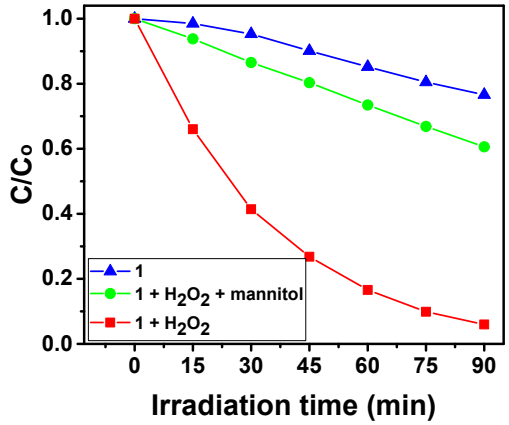

Fig. S32 Concentration changes of MB as a function of reaction time using catalyst **1** in the absence of H_2O_2, in the presence of H_2O_2, and in the presence of H_2O_2 and good hydroxyl radical (•OH) scavenger mannitol under visible light irradiation.

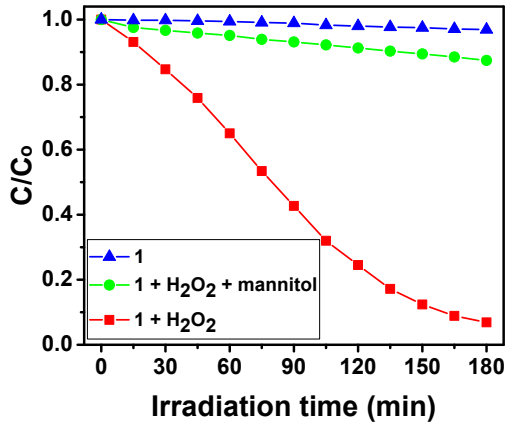

Fig. S33 Concentration changes of RhB as a function of reaction time using catalyst **1** in the absence of H_2O_2, in the presence of H_2O_2, and in the presence of H_2O_2 and good hydroxyl radical (•OH) scavenger mannitol under visible light irradiation.

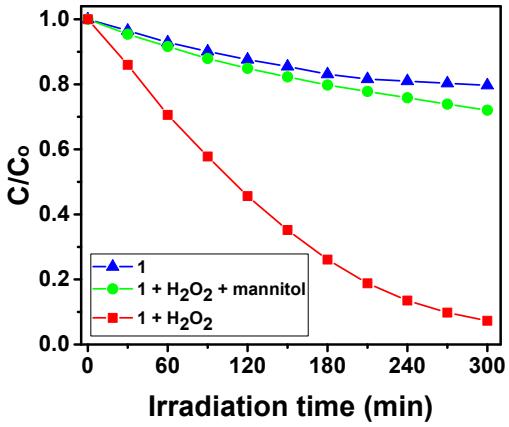

Fig. S34 Concentration changes of MO as a function of reaction time using catalyst **1** in the absence of H_2O_2, in the presence of H_2O_2, and in the presence of H_2O_2 and good hydroxyl radical (•OH) scavenger mannitol under visible light irradiation.